Journal of Radioanalytical and Nuclear Chemistry (2023) 332:3133–3145
https://doi.org/10.1007/s10967-023-08989-z

Prompt gamma rays from fast neutron induced reactions on cerium and chlorine

Niklas Ophoven[1,2] · Zeljko Ilic[1,3] · Eric Mauerhofer[1] · Tsitohaina H. Randriamalala[1] · Egor Vezhlev[1] · Christian Stieghorst[4] · Zsolt Révay[4] · Thomas Brückel[1,3] · Jan Jolie[2] · Erik Strub[2]

Received: 14 March 2023 / Accepted: 2 June 2023 / Published online: 1 July 2023

Abstract

Prompt gamma rays of cerium and chlorine were investigated with the FaNGaS (Fast Neutron-induced Gamma-ray Spectrometry) instrument operated at the Heinz Maier-Leibnitz Zentrum (MLZ) in Garching. The gamma radiation was emitted from (n,n'), (n,p) and (n,α) reactions induced by the irradiation of a cerium(III) chloride ($CeCl_3$) sample with a beam of fission neutrons. Additionally, a polyvinylchloride (PVC, $(C_2H_3Cl)_n$) sample was irradiated to verify possible interferences between gamma lines of cerium and chlorine. We identified 87 prompt gamma lines of cerium and chlorine. From these, we assigned 58 lines to the (n,n') reaction in cerium (one for ^{136}Ce, 41 for ^{140}Ce and 16 for ^{142}Ce), 23 to the (n,n') reaction in chlorine (15 for ^{35}Cl and 8 for ^{37}Cl), 5 lines to the ^{35}Cl(n,p)^{35}S reaction and 1 line to the ^{35}Cl(n,α)^{32}P reaction. We present relative intensities and fast-neutron spectrum-averaged partial cross sections of the aforementioned gamma lines and compare them with available literature data. Identification of new lines and discussion of possible errors adds important value to the literature data found to be consistent with our results. In addition, for a counting time of 12 h we estimate the detection limits for cerium and chlorine as 1 and 2 mg, respectively.

Keywords Inelastic scattering · Cerium · Chlorine · Fast neutron · Cross section · Gamma ray

Introduction

The advantages of using fast neutrons in non-destructive elemental analysis were demonstrated already several decades ago [1–5]. The FaNGaS (Fast Neutron-induced Gamma-ray Spectrometry) instrument [6–12], installed at Heinz Maier-Leibnitz Zentrum (MLZ) in 2014 and upgraded in 2020, advances this technique in neutron analytics and is available for a broad community of industry and research. At the FRM II (Forschungs-Neutronenquelle Heinz Maier-Leibnitz), the fast neutrons are produced using a highly-enriched uranium (93% ^{235}U) converter in the heavy water moderator. Passing through beamtube SR10, the beam enters the experimental room of the MEDAPP (Medical Application) instrument via a set of filters and collimators [13]. The electromechanically-cooled high-purity germanium (HPGe) detector is placed perpendicularly to the neutron beam. It is surrounded by a complex shielding against neutrons and gamma rays to reduce the spectral background. For the use of the FaNGaS instrument in nuclear analytical chemistry we are (i) continuously improving the instrument to further improve the peak-to-background ratio and (ii) building up a comprehensive data catalogue of (n,n'γ) reactions containing relative intensities and partial gamma-ray production cross sections for all natural elements. This catalogue is intended to update and extend the "Atlas of Gamma-rays from the Inelastic Scattering of Reactor Fast Neutrons", by Demidov et al. in 1978 [14], which is the only existing database for this reaction type [15–17]. However, while a database [18] exists based on [14] and a reasonable agreement compared to data evaluated from work at FRM II is generally observed, we also showed the need for a meticulous validation and

✉ Niklas Ophoven
n.ophoven@fz-juelich.de

1 Jülich Centre for Neutron Science, Forschungszentrum Jülich GmbH, 52425 Jülich, Germany

2 Mathematisch-Naturwissenschaftliche Fakultät, Universität zu Köln, 50923 Cologne, Germany

3 Lehrstuhl Für Experimentalphysik IVc, RWTH Aachen University, 52056 Aachen, Germany

4 Heinz Maier-Leibnitz Zentrum (MLZ), Technische Universität München, Lichtenbergstraße 1, 85748 Garching, Germany

reevaluation of the data in our former publications [6–12]. Furthermore, the measurements performed at FRM II provide a valuable contribution to the nuclear data community with new gamma-ray data from an alternative fission source with an average incident neutron energy closer to that one expected from a fission spectrum and much higher than in Demidov's work.

In the present work, we provide the results from the measurement of prompt gamma rays induced by (n,n') inelastic scattering and (n,p) and (n,α) reactions on cerium and chlorine. The measurements were performed with an upgraded version of the FaNGaS instrument as described in [12]. In order to check if the cerium(III) chloride ($CeCl_3$) sample is free of water and to exclude interferences between chlorine and cerium we also report on the measurement of a polyvinylchloride (PVC, $(C_2H_3Cl)_n$) sample. Relative gamma-ray intensities and fast-neutron spectrum-averaged partial gamma-ray production cross sections are presented including comparisons with available literature data. In addition, we also give elemental detection limits for cerium and chlorine.

Experimental

Prompt gamma radiation induced by fast neutrons on a $CeCl_3$ powder sample (mass: 2.66 g, Ce: 1.51 g, Cl: 1.15 g) and on a PVC foil (mass: 0.15 g, Cl: 0.08 g, C: 0.06 g, H: 0.01 g) was investigated with the FaNGaS instrument described in [12]. The $CeCl_3$ powder was filled into a small PTFE (Polytetrafluorethylene) bag. The maximum thickness of the sample was estimated to be 5 mm. The thickness of the PVC foil was 0.2 mm. The samples were attached to a thin PTFE rod as the sample holder, and the samples were tilted by an angle of 45° with respect to the beam direction. They were completely irradiated by the fast neutrons with a flux at sample position of $(1.13 \pm 0.04) \times 10^8$ cm^{-2} s^{-1} and an average neutron energy of 2.30 MeV. The irradiation time was 3.4 h for $CeCl_3$ and 17 h for PVC, and the live times were 2.7 and 15.4 h, respectively, meaning 20% and 10% deadtimes, respectively. The measurement was performed at a sample-to-detector distance of 67 cm and at an angle of 90° to the beam direction. The acquired spectra were analyzed with the HYPERMET-PC software [19] and they are shown in Figs. 1 and 2. Prompt gamma rays emitted from the (n,n') inelastic scattering as well as (n,p) and (n,α) reactions of fast neutrons were identified using the NuDat 3.0 database [20] and associated nuclear data from various evaluations for all nuclides relevant to this work [21–27]. Presence of gamma rays from (n,γ) reactions and possible interferences were checked with the prompt gamma neutron activation analysis (PGNAA) database [28].

As a certain fraction of neutrons scatters towards the spectrometer, we have observed an increase of the count rate of the background lines. For the $CeCl_3$ sample, we found a mean factor of 1.42 ± 0.30, while for the PVC sample 1.03 ± 0.10. In the case of $CeCl_3$ this scattering factor was used to correct for the interfering background lines, whereas it could be neglected for PVC. Correction for interferences arising from a single or double escape peak (denoted as SE and DE, respectively) is discussed in the following section.

Method

Inelastic neutron scattering reactions have threshold energies typically above 100 keV. This is mostly true also for (n,p) and (n,α) reactions with the exception of a few light nuclides for which no thresholds are observed [29, 30]. The net peak area $P_{E\gamma}$ of a prompt gamma ray emitted from the aforementioned reactions can be described by the following relationship [9–12]:

$$P_{E\gamma}(90°) = \frac{m}{M} \cdot N_A \cdot h \cdot \varepsilon_{E\gamma} \cdot \langle \sigma_{E\gamma}(90°) \rangle \cdot \langle \Phi_{fast} \rangle \cdot t_c \cdot f_n \cdot f_{E\gamma} \quad (1)$$

where m (g) is the mass of the considered element, M is the molar mass (g mol^{-1}), N_A the Avogadro constant (6.022×10^{-23} mol^{-1}), h the isotopic abundance, $\varepsilon_{E\gamma}$ the full-energy-peak (FEP) efficiency, $<\sigma_{E\gamma}(90°)>$ the fast-neutron spectrum-averaged partial gamma-ray production cross section (cm^2) for an angle of 90° between neutron beam and detector, $<\Phi_{fast}>$ the integral fast neutron flux (cm^{-2} s^{-1}), t_c the counting live time (s), f_n the neutron self-shielding factor and $f_{E\gamma}$ the gamma-ray self-absorption factor. The PVC sample is thin enough to neglect the self-attenuation factors, i.e. $f_n \sim 1$ and $f_{E\gamma} \sim 1$. The neutron self-shielding of the $CeCl_3$ sample was investigated by numerical simulation using the Monte Carlo N-Particle (MCNP, version 6.1) [31, 32] code. The Lib80x library [33] with ENDF/B-VIII.0 data was used [34]. The irradiation of a $CeCl_3$ slab of 5 mm thickness, tilted by an angle of 45° and having a mass equal to the one of our measurement, was simulated with a neutron-energy distribution identical to our experiment. The neutron self-shielding factor is determined as the ratio of the average fast neutron flux within the sample (F4 tally) to the incident fast neutron flux on the sample (F2 tally). The value of $f_n = 1.01$ indicates that the neutron self-shielding can be neglected.

The gamma-ray self-absorption factor $f_{E\gamma}$ for the $CeCl_3$ sample can be analytically calculated as [28, 35]:

$$f_{E\gamma} = \frac{1 - e^{-\frac{\mu}{\rho} \cdot \rho \cdot l}}{\frac{\mu}{\rho} \cdot \rho \cdot l} \quad (2)$$

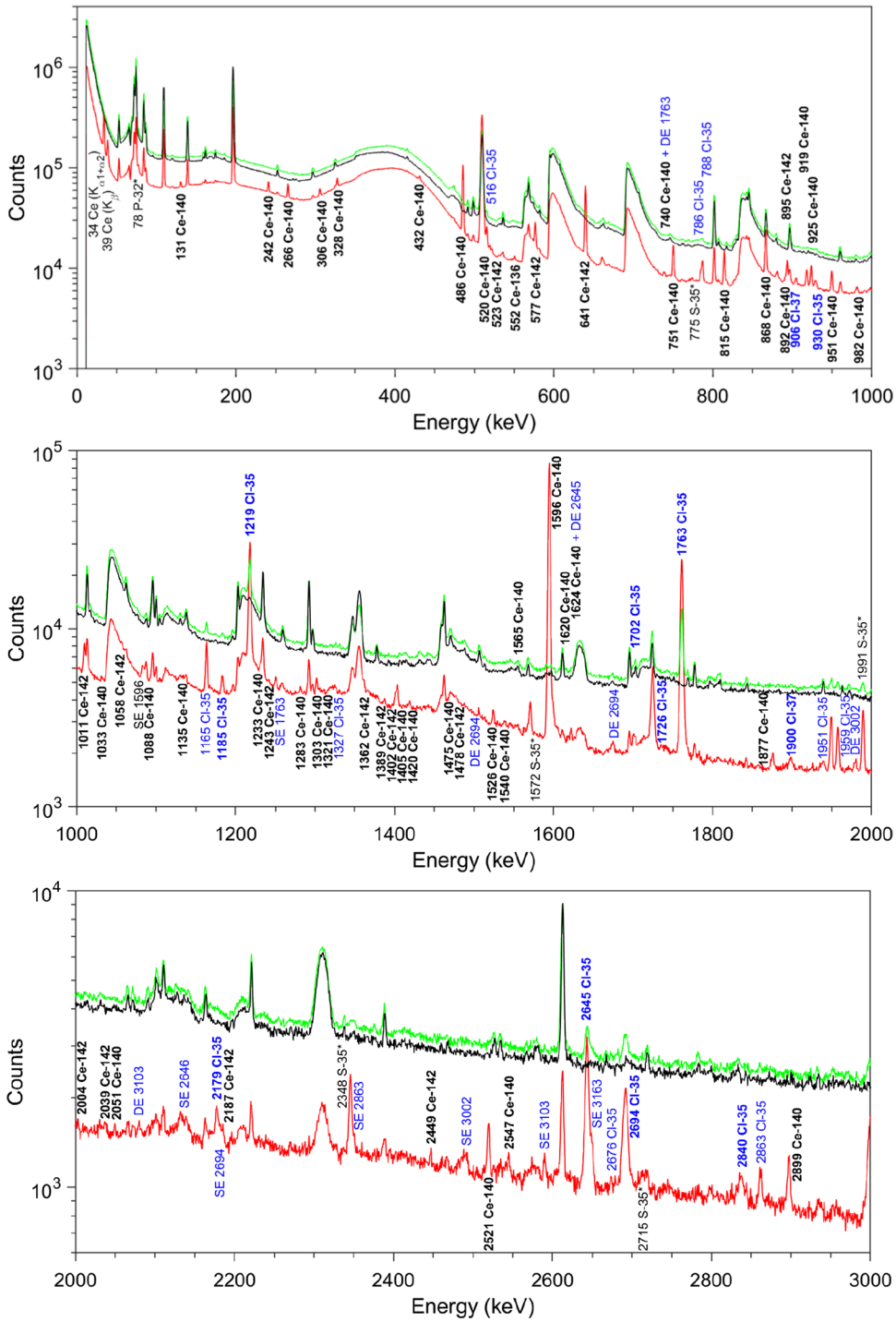

Fig. 1 Gamma-ray spectra in the energy range 0–3000 keV acquired during 55,478 s counting live time for the PVC sample (green), 9743 s for the $CeCl_3$ sample (red) and during 51,506 s for the beam background (black). Prompt gamma rays induced by (n,p) reactions (S-35) and (n,α) reactions (P-32) on Cl-35 are written in black with an asterisk. Other lines marked in black but without an asterisk represent X-rays from cerium. Prompt gamma rays issued from (n,n') inelastic scattering of fast neutrons on cerium are written in black and bold. They are written in bold blue for the case of chlorine. Lines in light blue are capture gamma rays from Cl-35. Abbreviations SE and DE indicate single and double escape peaks, respectively. The origin of prominent lines attributed to the beam background is discussed within our former publications [7, 9]. (Color figure online)

where $l = 0.71$ cm is the effective thickness of the sample, μ/ρ (cm^2 g^{-1}) denotes the mass attenuation coefficient (cm^2 g^{-1}) and $\rho = 3.97$ g cm^{-3} is the density of the sample. The total value of μ/ρ including coherent scattering was taken from the NIST (National Institute of Standards and Technology) photon cross sections database XCOM [36, 37]. The $f_{E\gamma}$ values were determined with Eq. (2) for various discrete energies between 100 and 5000 keV. The dependence of the gamma-ray self-absorption factors $f_{E\gamma}$ on the gamma-ray energy E_γ is shown in Fig. 3. The data points were fitted with the following semi-empirical function:

$$f_{E\gamma} = a_0 + a_1 \cdot \left(1 - e^{-a_2 \cdot E_\gamma}\right) + a_3 \cdot \left(1 - e^{-a_4 \cdot E_\gamma}\right) \quad (3)$$

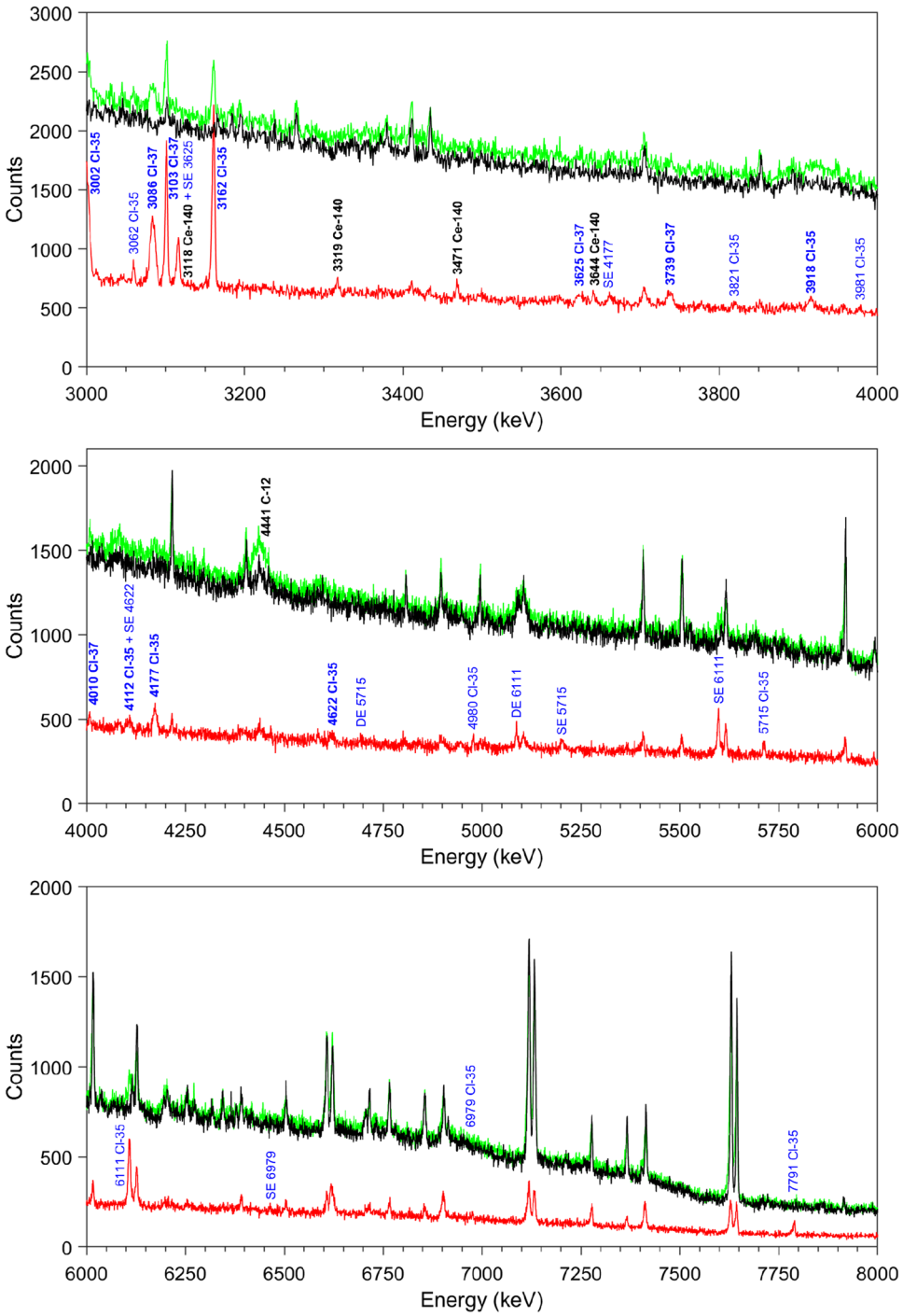

Fig. 2 Gamma-ray spectra in the energy range 3000–8000 keV acquired during 55,478 s counting live time for the PVC sample (green), 9,743 s for the $CeCl_3$ sample (red) and during 51,506 s for the beam background (black). Prompt gamma rays issued from (n,n') inelastic scattering of fast neutrons on cerium are written in black and bold. They are written in bold blue for the case of chlorine. Lines in light blue are capture gamma rays from Cl-35. Abbreviations SE and DE indicate single and double escape peaks, respectively. The prompt line of C-12 was observed in the PVC measurement. The origin of prominent lines attributed to the beam background is discussed within our former publications [7, 9]. (Color figure online)

with $a_0 = -1.1265 \pm 0.0546$, $a_1 = 0.1368 \pm 0.0142$, $a_2 = 0.0014 \pm 0.0002$, $a_3 = 1.9425 \pm 0.0449$, $a_4 = 0.0118 \pm 0.0003$ and E_γ in units of keV.

For the correction of SE and DE interferences the energy deposited by high-energy gammas in the HPGe detector was simulated using the F8 tally of the MCNP code [31, 32]. Based on the technical drawing provided by the manufacturer (ORTEC®), a realistic detector model was implemented in the simulation. The gamma source was defined as a parallel photon beam of several discrete energies between 1.3 and 8.0 MeV. The ratios between net counts of SEs and FEPs and between net counts of DEs and FEPs were deduced from the simulated spectrum. The dependence of the logarithmic value of the ratios on the gamma energy is shown in Fig. 4 and was approximated with Eq. (4):

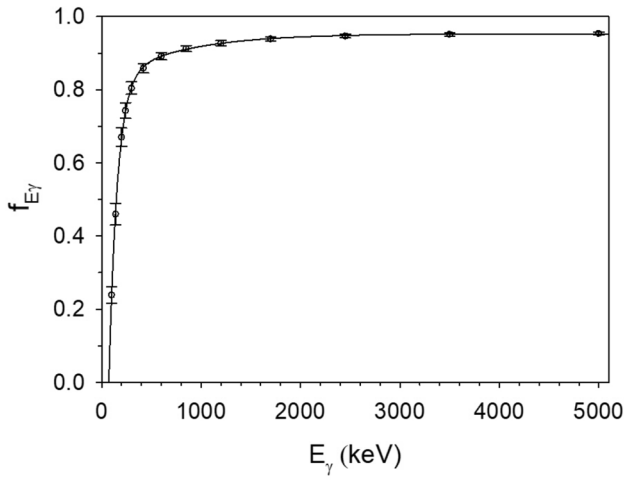

Fig. 3 Dependence of the gamma-ray self-absorption factor $f_{E\gamma}$ on the gamma energy E_γ. The solid line represents the fit of the data taken from NIST XCOM [36, 37] with Eq. (3)

$$\log\left(\frac{\mathrm{SE}}{\mathrm{FEP}}\right)\text{or}\log\left(\frac{\mathrm{DE}}{\mathrm{FEP}}\right) = b_0 + \left(\frac{b_1}{E_\gamma}\right) + \left(\frac{b_2}{E_\gamma^2}\right) + \left(\frac{b_3}{E_\gamma^3}\right) \quad (4)$$

with $b_0 = 0.7737 \pm 0.0385$, $b_1 = (-6.3758 \pm 0.3493) \cdot 10^3$, $b_2 = (7.3210 \pm 0.8957) \cdot 10^6$, $b_3 = (-6.2095 \pm 0.6781) \cdot 10^9$ for SE correction and $b_0 = 0.4463 \pm 0.0432$, $b_1 = (-6.3979 \pm 0.3912) \cdot 10^3$, $b_2 = (7.4241 \pm 1.0031) \cdot 10^6$, $b_3 = (-6.1875 \pm 0.7594) \cdot 10^9$ for DE correction with E_γ in units of keV. The calculated values are in good agreement with the experimental ones (see Fig. 4).

Prompt gamma rays of chlorine

Twenty nine gamma lines from the interaction of fast neutrons with chlorine were identified in the $CeCl_3$ spectrum, 15 assigned to the $^{35}Cl(n,n')^{35}Cl$, 8 to the $^{37}Cl(n,n')^{37}Cl$, 5 to the $^{35}Cl(n,p)^{35}S$ and 1 to the $^{35}Cl(n,\alpha)^{32}P$ reaction, respectively (see Table 1). In the case of the PVC sample, only 14 fast-neutron-induced lines were measured, 7 related to the $^{35}Cl(n,n')^{35}Cl$, 4 to the $^{37}Cl(n,n')^{37}Cl$ and 3 to the $^{35}Cl(n,p)^{35}S$ reaction. The lower number of observed gamma rays in the PVC spectrum is explained with the lower sensitivity stemming from the much smaller sample mass only partly compensated by the longer measurement time. Since PVC contains carbon we also measured the Doppler-broadened [38, 39] gamma ray of the $^{12}C(n,n'\gamma)^{12}C$ reaction. Additionally, in both spectra, the main neutron capture lines of chlorine were identified as our neutron spectrum contains epithermal and thermal neutrons [9, 10, 12]. No significant interferences between the capture lines and the fast-neutron-induced lines of chlorine were observed. The PVC foil was also used to check the composition and absence of crystal water in the $CeCl_3$ sample, as the chlorine peak count rate ratios were found to agree with the nominal chlorine mass ratio. The interference-free (according to [20]) lines at 2645 and 3002 keV from the $^{35}Cl(n,n'\gamma)^{35}Cl$ reaction yielded an average chlorine mass of (1.14 ± 0.05) g, which is in good agreement with the value calculated from the nominal composition of the chloride (1.15 g). Therefore, the sample is assumed to contain no water as the hexahydrate would yield a chlorine mass of 0.80 g.

Intensities of the gamma lines were calculated relative to the 1219-keV line of ^{35}Cl. They are compared

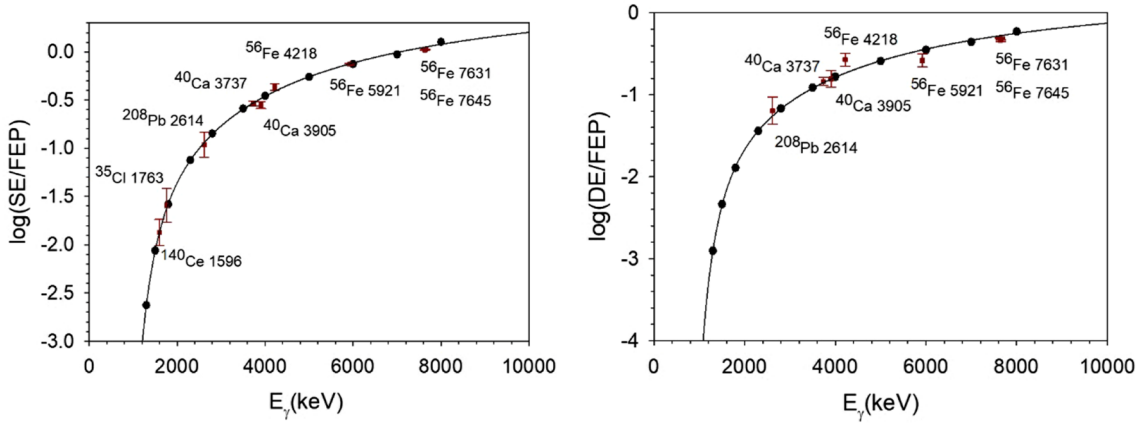

Fig. 4 Determined correction curves for single (left) and double (right) escape peak interferences. Round values in black represent data points obtained with MCNP, the solid line in black is the curve fit with the function given in Eq. (4). Square dots in red with error bars represent experimental values. Values from the isotopes ^{35}Cl and ^{140}Ce were determined from the $CeCl_3$ measurement described in this work (see also Figs. 1 and 2), values of ^{40}Ca are from our previous measurement of $CaCO_3$ [12] and values from ^{208}Pb and ^{56}Fe are taken from the beam background [7, 9]

Table 1 Prompt gamma rays of ^{35}Cl and ^{37}Cl induced by fast neutrons on $CeCl_3$

Reaction (E_{thr})	This work				From Demidov Atlas [14]		R
	E_γ (keV)	$P_{E\gamma}(90°)/(\varepsilon_{E\gamma}{\cdot}f_{E\gamma})\times10^{-8}$ (count)	I_R(relative) (%)	$<\sigma_{E\gamma}(90°)>$ (mb)	E_γ (keV)	I_R(relative) (%)	
$^{35}Cl(n,n'\gamma)^{35}Cl$ (1.25 MeV)	930.29 ± 0.10[a]	0.37 ± 0.08	3.16 ± 0.72	**2.26 ± 0.51**	930.5 ± 0.5	3.0 ± 1.0	0.13
	1184.64 ± 0.08	0.47 ± 0.03	4.03 ± 0.30	**2.89 ± 0.19**	1184.72 ± 0.15[b]	3.8 ± 0.4	0.47
	1219.25 ± 0.06[c]	11.62 ± 0.35	100	72 ± 2	1219.52 ± 0.10	100	–
	1701.73 ± 0.14[a]	0.12 ± 0.04	1.06 ± 0.34	**0.76 ± 0.24**	–	–	–
	1762.92 ± 0.08[d]	13.26 ± 0.43	114 ± 5	82 ± 3	1763.27 ± 0.10	129 ± 4	−2.31
	2179.10 ± 0.21	0.37 ± 0.03	3.22 ± 0.28	**2.31 ± 0.19**	2180.8 ± 0.3[e]	6.2 ± 0.6	−4.50
	2645.20 ± 0.12	2.51 ± 0.11	21.6 ± 1.2	15.4 ± 0.7	2645.7 ± 0.2	25.7 ± 1.5	−2.19
	2693.78 ± 0.13[a,f]	2.03 ± 0.63	17.4 ± 5.4	**12.5 ± 3.9**	2694.0 ± 0.2	19.1 ± 1.5	−0.30
	2839.60 ± 0.39[f]	0.25 ± 0.03	2.11 ± 0.26	**1.51 ± 0.18**	2840.3 ± 0.4[e]	5.4 ± 0.6	−5.02
	3002.32 ± 0.12[f]	2.04 ± 0.09	17.6 ± 0.9	**12.6 ± 0.5**	3002.2 ± 0.2	15.5 ± 1.5	1.17
	3162.46 ± 0.11	1.68 ± 0.06	14.4 ± 0.7	10.3 ± 0.4	3162.52 ± 0.15	16.3 ± 1.5	−2.65
	3918.46 ± 0.47[f]	0.12 ± 0.02	1.05 ± 0.17	**0.75 ± 0.12**	–	–	–
	4110.81 ± 0.25[g]	0.27 ± 0.05	2.30 ± 0.43	**1.65 ± 0.31**	–	–	–
	4176.65 ± 0.75[i]	0.61 ± 0.05	5.22 ± 0.46	**3.74 ± 0.31**	–	–	–
	4622.17 ± 0.23[f]	0.30 ± 0.04	2.61 ± 0.38	**1.87 ± 0.27**	–	–	–
$^{37}Cl(n,n'\gamma)^{37}Cl$ (1.77 MeV)	905.65 ± 0.08	0.29 ± 0.02	2.53 ± 0.20	5.66 ± 0.41	906.64 ± 0.15	2.9 ± 0.4	−0.83
	1726.17 ± 0.08[a,d,h]	2.38 ± 0.09	20.5 ± 1.0	46 ± 2	1726.50 ± 0.10	25 ± 2	−2.01
	1899.99 ± 0.28[f,h]	0.12 ± 0.03	1.06 ± 0.25	**2.38 ± 0.56**	–	–	–
	3085.91 ± 0.14[f]	1.17 ± 0.05	10.0 ± 0.5	22 ± 1	3086.3 ± 0.3	11.2 ± 1.0	−1.02
	3103.17 ± 0.11[a]	1.29 ± 0.05	11.1 ± 0.5	25 ± 1	3103.29 ± 0.15	14.6 ± 1.5	−2.17
	3625.48 ± 0.90[f]	0.24 ± 0.04	2.07 ± 0.34	**4.65 ± 0.74**	–	–	–
	3739.47 ± 0.18[f]	0.31 ± 0.04	2.65 ± 0.32	**5.93 ± 0.68**	3742.9 ± 0.5	3.0 ± 1.0	−0.33
	4010.3 ± 0.32	0.16 ± 0.02	1.37 ± 0.20	**3.08 ± 0.43**	–	–	–
$^{35}Cl(n,p)^{35}S$ (0 MeV)	774.83 ± 0.18[h,j]	0.07 ± 0.02	0.62 ± 0.17	**0.45 ± 0.12**	775.0 ± 0.2	1.3 ± 0.3	−1.95
	1572.05 ± 0.10[a]	0.65 ± 0.04	5.57 ± 0.38	**3.99 ± 0.25**	1572.32 ± 0.13	5.9 ± 0.5	−0.52
	1990.92 ± 0.09	1.19 ± 0.04	10.2 ± 0.5	**7.33 ± 0.25**	1991.43 ± 0.15	11.6 ± 1.0	−1.23
	2347.617 ± 0.11[h]	0.51 ± 0.04	4.39 ± 0.35	3.14 ± 0.23	2347.9 ± 0.4	6.6 ± 0.6	−3.19
	2714.90 ± 0.50[f]	0.10 ± 0.02	0.82 ± 0.20	**0.59 ± 0.15**	–	–	–
$^{35}Cl(n,\alpha)^{32}P$ (0 MeV)	77.97 ± 0.06[k]	5.17 ± 0.54	45 ± 5	**32 ± 3**	–	–	–

E_{thr} is the threshold energy of the considered reaction taken from [29, 30], E_γ is the gamma-ray energy, $P_{E\gamma}(90°)/(\varepsilon_{E\gamma}{\cdot}f_{E\gamma})$ the net counts in the gamma-ray peak divided by the full-energy-peak efficiency and the gamma self-absorption factor, I_R the relative intensity of the gamma ray and $<\sigma_{E\gamma}(90°)>$ the fission-neutron spectrum-averaged partial cross section for gamma-ray production at an angle of 90° between neutron beam and detector determined with Eq. (1). R is the residual calculated by means of Eq. (6). Cross sections written in bold are proposed

[a]Corrected for background interferences

[b]Unassigned by Demidov et al.

[c]Negligible interference from the $^{140}Ce(n,n'\gamma)^{140}Ce$ reaction [26], but interference unreported on [20] is assumed as the cross section differs much compared to that given in Table 2

[d]Possible interference from the $^{142}Ce(n,n'\gamma)^{142}Ce$ reaction [27]

[e]Maybe uncorrected interference in [14] from the SE from the 2693.8-keV line of ^{35}Cl

[f]Doppler-broadened; short-lived transitions in the femtosecond range [21–23]

[g]Corrected for contribution of SE from 4622 keV (32.6% of total counts)

[h]Interference from $^{140}Ce(n,n'\gamma)^{140}Ce$ reaction corrected with relative intensities given in the ENSDF file [26] on [20]

[i]Might be fed from two close-lying short-lived levels; possible, but unlikely to come from $^{37}Cl(n,n'\gamma)^{37}Cl$ reaction [22]

[j]Data from Demidov et al. might be more accurate due to a higher chlorine mass and counting time [14]

[k]Considerable self-absorption with $f_{E\gamma}=0.128\pm0.013$, calculated after Eq. (2)

to the values by Demidov et al. [14] in columns 4 and 7 of Tables 1 and 2. We detected 19 out of 27 lines given in [14], of which only 21 were originally assigned to fast-neutron reactions. The lines listed at 637.2, 824.8, 882.3, 922.0, 1070.6, 1676.4, 2832.9 and 3195.9 keV in [14] were not observed in our measurements. The line at 882.3 keV was not identified due to interference with the 881-keV line of ^{206}Pb induced by inelastic scattering of fast neutrons with the lead shielding [9]. The lines at 637.2 and 1070.6 keV were not detected due to the low mass of the samples. The lines at 824.8, 922.0, 1676.4, 2832.9 and 3195.9 keV were reported as tentative assignments by Demidov et al. and were not placed in any chlorine decay scheme. They are not observed in our measurements, so they most likely do not belong to chlorine. It should be mentioned that according to [20, 23] the 1676.4-keV line could be emitted from an excited level at $E^* = 1755.0$ keV of ^{32}P. The 3195.9-keV line could correspond to the SE of a line at 3707.9 keV directly emitted to ground sate (g.s.) in ^{37}Cl [20, 22]. The clear presence of the 3195.9-keV line in the spectrum of Demidov et al., which is shown only to 3.5 MeV, together with the absence of a reasonable transition in [20] might support this assumption.

On the other hand, compared to [14] we identify 10 new gamma lines of chlorine that are also reported in [20]. These include the lines at 1701.7, 3918.5, 4110.8, 4176.7 and 4622.2 keV for the ^{35}Cl(n,n')^{35}Cl, the lines at 1900.0, 3625.5 and 4010.3 for the ^{37}Cl(n,n')^{37}Cl, the line at 2714.9 keV for the ^{35}Cl(n,p)^{35}S and the line at 78.0 keV for the ^{35}Cl(n,α)^{32}P reaction (see also Figs. 1 and 2). Another gamma ray at 1184.6 keV, listed but unassigned in [14], was found to belong to the ^{35}Cl(n,n')^{35}Cl reaction.

For the lines at 774.8, 1726.2, 1900.0 and 2347.6 keV in the $CeCl_3$ spectrum, Demidov et al. suggest interferences with lines from the ^{140}Ce(n,n'γ)^{140}Ce reaction. They were corrected using the relative intensities in the evaluated nuclear structure data file (ENSDF) [26] for the corresponding (n,n'γ) reaction, because a large discrepancy in intensity compared to the original work of [14] for those lines was observed. The contributions from the interfering (n,n'γ)

Table 2 Prompt gamma rays of ^{35}Cl, ^{37}Cl and ^{12}C induced by fast neutrons on PVC

Reaction (E_{thr})	This work				From Demidov Atlas [14]		R
	E_γ (keV)	$P_{E\gamma}(90°)/\varepsilon_{E\gamma} \times 10^{-8}$ (count)	I_R(relative) (%)	$<\sigma_{E\gamma}(90°)>$ (mb)	E_γ (keV)	I_R(relative) (%)	
^{35}Cl(n,n'γ)^{35}Cl (1.25 MeV)	1184.94 ± 0.16	0.17 ± 0.03	4.31 ± 0.69	2.51 ± 0.44	1184.72 ± 0.15[a]	3.8 ± 0.4	0.65
	1219.32 ± 0.05	3.87 ± 0.14	100	**58 ± 5**	1219.52 ± 0.10	100	–
	1763.05 ± 0.07	4.62 ± 0.15	119 ± 6	**70 ± 6**	1763.27 ± 0.10	129 ± 4	−1.36
	2646.08 ± 0.16	0.98 ± 0.05	25.3 ± 1.6	**14.7 ± 1.4**	2645.7 ± 0.2	25.7 ± 1.5	−0.19
	2694.35 ± 0.18[b,c]	0.64 ± 0.15	16.5 ± 3.9	9.58 ± 2.35	2694.0 ± 0.2	19.1 ± 1.5	−0.64
	3002.46 ± 0.55	0.79 ± 0.08	20.4 ± 2.1	11.9 ± 1.5	3002.2 ± 0.2	15.5 ± 1.5	1.92
	3162.76 ± 0.13	0.59 ± 0.05	15.3 ± 1.3	**8.92 ± 0.98**	3162.52 ± 0.15	16.3 ± 1.5	−0.49
^{37}Cl(n,n'γ)^{37}Cl (1.77 MeV)	905.78 ± 0.39	0.11 ± 0.03	2.89 ± 0.82	**5.27 ± 1.54**	906.64 ± 0.15	2.9 ± 0.4	−0.01
	1725.60 ± 0.19[b]	0.79 ± 0.05	20.6 ± 1.3	**37 ± 4**	1726.50 ± 0.10	25 ± 2	−1.87
	3086.3 ± 0.55[c]	0.46 ± 0.10	12.0 ± 2.6	**22 ± 5**	3086.3 ± 0.3	11.2 ± 1.0	0.28
	3103.24 ± 0.18[b]	0.46 ± 0.08	11.8 ± 2.2	**22 ± 4**	3103.29 ± 0.15	14.6 ± 1.5	−1.04
^{35}Cl(n,p)^{35}S (0 MeV)	1572.83 ± 0.33	0.20 ± 0.03	5.17 ± 0.78	3.01 ± 0.50	1572.32 ± 0.13	5.9 ± 0.5	−0.79
	1991.02 ± 0.17	0.34 ± 0.04	8.73 ± 1.05	5.08 ± 0.71	1991.43 ± 0.15	11.6 ± 1.0	−1.98
	2348.54 ± 0.37[c]	0.17 ± 0.03	4.41 ± 0.77	**2.57 ± 0.48**	2347.9 ± 0.4	6.6 ± 0.6	−2.24
^{12}C(n,n'γ)^{12}C (4.81 MeV)[d]	4440.96 ± 0.15[b,c]	2.22 ± 0.37	100	12.8 ± 2.3	4438 ± 2	109[e]	–

E_{thr} is the threshold energy of the considered reaction taken from [29, 30], E_γ is the gamma-ray energy, $P_{E\gamma}(90°)/\varepsilon_{E\gamma}$ the net counts in the gamma-ray peak divided by the full-energy-peak efficiency, I_R the relative intensity of the gamma ray and $<\sigma_{E\gamma}(90°)>$ the fission-neutron spectrum-averaged partial cross section for gamma-ray production at an angle of 90° between neutron beam and detector determined with Eq. (1). R is the residual calculated by means of Eq. (6). Cross sections written in bold are proposed

[a]Unassigned by Demidov et al.

[b]Corrected for background interferences

[c]Doppler-broadened; short-lived transitions in the femtosecond range [21–23, 38]

[d]Only elemental data available from [29, 30]

[e]Unclear how this intensity is obtained, it might be a mistake or the absolute intensity determined with the integral cross section. From our work the absolute intensity is 107% by using an integral cross section for fission neutrons of roughly 12 mb [40] with an angular distribution correction factor of $W(90°) = 1$

reaction to the net counts were calculated as (32.0 ± 5.3)%, (3.7 ± 0.3)%, (17.2 ± 3.1)% and (44.2 ± 2.7)%, respectively.

The correlation between the relative intensities in this work and in [14] is depicted in Fig. 5 for our two measurements. The values have been fitted with the following semi-empirical function [10–12]:

$$I_R = a \cdot \left(I_{RD}\right)^b \tag{5}$$

with $a = 0.68 \pm 0.10$ and $b = 1.07 \pm 0.06$ for the $CeCl_3$, and $a = 0.94 \pm 0.14$ and $b = 0.99 \pm 0.06$ for the PVC sample.

The average intensity ratios I_R/I_{RD} of 0.83 ± 0.19 ($CeCl_3$) and I_R/I_{RD} of 0.94 ± 0.16 (PVC) indicate a good agreement between the two measurements. To prove the consistency in a more detailed manner, Fig. 6 shows the two sets of data in the form of a common histogram of the residuals R in units of standard deviation [σ] for our two measurements, calculated as [10–12]:

$$R = \frac{I_R - I_{RD}}{\sqrt{\left(s_{I_R}\right)^2 + \left(s_{I_{RD}}\right)^2}} \tag{6}$$

The fit of the data agrees at the 1.3σ level and the Gaussian centroid is shifted by −1.002, indicating a systematic effect. We assume that the large shift mainly originates from the lines at 774.8, 2179.1 and 2839.6 keV, only observed in the $CeCl_3$ sample. For these lines we found much less intensity compared to [14].

The fast-neutron spectrum-averaged partial cross sections for gamma-ray production calculated by means of Eq. (1) are given in column 5 of Tables 1 and 2. The values of the two datasets agree well with each other, taking into account the uncertainties except for the lines at 1219, 1572, 1726, 1763 and 1991 keV. For the latter the cross sections obtained from the $CeCl_3$ measurement are roughly higher by factors between 1.2 and 1.4 than these derived from the PVC measurement, thus, indicating possible interferences from cerium lines. For the line at 1219 keV we propose the cross section obtained from the PVC irradiation, while for all others the cross sections with the better R value, i.e. greater agreement in relative intensity with [14], are suggested. Proposed cross sections are written in bold in Tables 1 and 2.

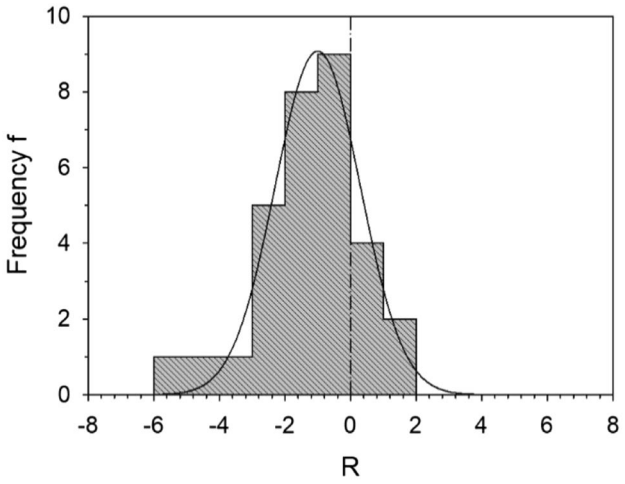

Fig. 6 Comparison of the relative intensities of the prompt gamma rays induced by fast-neutron inelastic scattering (n,n'), (n,p) and (n,α) reactions on chlorine obtained in this work with the data tabulated in the Demidov Atlas [14] in the form of a histogram of the residuals R in units of standard deviation [σ] calculated with Eq. (6). The plot represents data from both the $CeCl_3$ and PVC spectrum. The values of R are given in column 8 of Tables 1 and 2. The solid line represents the fit of the data with a Gaussian

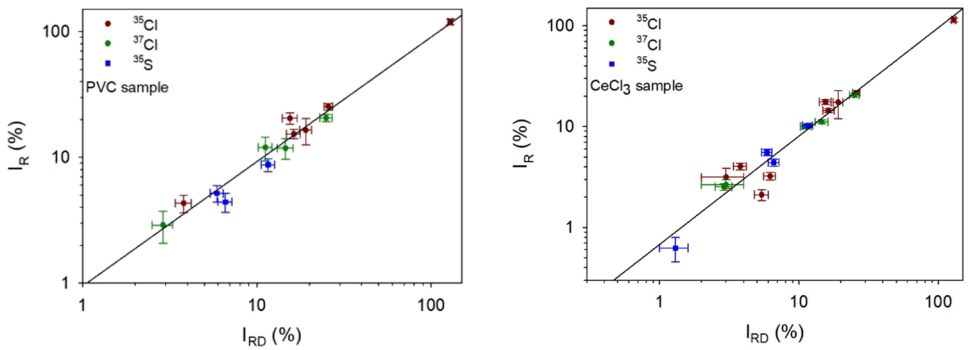

Fig. 5 Relationship between the relative intensities I_R of the prompt gamma rays induced by fast-neutron inelastic scattering (n,n') and (n,p) reactions on chlorine measured in this work and the relative intensities I_{RD} tabulated in the Demidov Atlas [14]. The left plot represents data from the PVC spectrum whereas the right plot was obtained with data from the $CeCl_3$ spectrum. The solid line represents the fit of the data with Eq. (5)

Prompt gamma rays of cerium

Fifty eight gamma lines from inelastic scattering of fast neutrons on cerium were found, one related to ^{136}Ce, 41 to ^{140}Ce and 16 to ^{142}Ce. These gamma rays are depicted in Figs. 1 and 2 and their data are given in Tables 3 and 4. No neutron capture lines from cerium were identified.

Intensities of gamma lines were calculated relative to the 1596-keV line of ^{140}Ce. They are given along with the values determined in [14] in columns 3 and 6 of Tables 3 and 4. We detected 31 out of 45 lines given in [14], of which only 27 lines were originally assigned to fast-neutron reactions. The gamma rays listed at energies of 337.0, 740.0, 774.0, 788.2, 846.3, 983.1, 1041.1, 1045.5, 1059.0, 1098.8, 1233.6, 1463.3, 1526.4, 1620.5, 1724.9, 1812.3, 1899.3 and 1958.5 keV in Demidov's Atlas are reported as tentative assignments and are unplaced in the decay schemes of cerium isotopes. The lines at 740.0, 983.1, 1059.0, 1233.6, 1526.4 and 1620.5 were observed in the current work and assigned based on data provided in [20]. The 337.0-, 846.3-, 1041.1-, 1463.3- and 1958.5-keV lines are not specified in [20, 24–27] and the placement of the line at 1812.3 keV in the level scheme of ^{140}Ce is uncertain [20, 26]. In our measurement the lines at 337.0, 846.3, 962.2, 1041.1, 1045.5, 1098.8 and 1463.3 keV were not observed uniquely due to interferences with background lines [7, 9]. The lines at 788.2 and 1958.5 keV are mainly associated to the neutron capture lines of ^{35}Cl and the lines at 774.8 and 2347.5 keV are essentially issued from the ^{35}Cl(n,p)^{35}S reaction. The 1724.9-keV line was not identified uniquely due to strong interferences with the 1726.2-keV line of ^{37}Cl and the background lines of ^{207}Pb and ^{56}Fe at 1725 keV [9]. The line at 1899.3 keV listed in [14] is mainly related to the 1900.0-keV line of ^{37}Cl.

The DEs of the lines at 1762.9 keV (^{35}Cl) and 2645.2 keV (^{35}Cl) as well as the SE of the line at 3625.5 keV (^{37}Cl) were found to interfere significantly with the lines at 739.6, 1623.6 and 3118.2 keV, respectively. Their contributions to the net count rates were estimated with Eq. (4) to be (34.9 ± 3.3)%, (41.9 ± 4.9)% and (14.5 ± 2.5)%, respectively. The contribution of the DE of the background line at 2614 keV (^{208}Pb) [7, 9] to the net count rate of the 1596.0-keV line is negligible with (0.11 ± 0.02)%. The lines of ^{140}Ce mentioned at 1085 and 1252 keV in [20, 26] are identified as escape peaks of the 1596.0-keV line of ^{140}Ce and the 1762.9-keV-line of ^{35}Cl with contributions of (99.3 ± 7.3)% and (94.0 ± 10.3)%, respectively.

On the other hand, in comparison to [14] we have identified 27 new gamma lines (one for ^{136}Ce, 17 for ^{140}Ce and 9 for ^{142}Ce) which are all specified in [20]. Because of the better energy resolution of our detector it was possible to resolve doublets in the lines given by Demidov et al. at energies of 522.0, 894.8 and 1404.3 keV (see Tables 3 and 4).

The correlation between the relative intensities measured in this work and these given in [14] is depicted in Fig. 7 for all lines. The values have been fitted with Eq. (5) yielding the coefficients $a = 0.86 \pm 0.06$ and $b = 0.98 \pm 0.05$. The average intensity ratio I_R/I_{RD} is 0.93 ± 0.23, indicating a reasonable agreement between the two measurements.

Figure 8 shows the two sets of data in the form of a histogram of the residuals R in units of standard deviation [σ], calculated according to Eq. (6). The fit of the data agrees at the 1.2σ level and the Gaussian centroid is shifted by −0.671, indicating a probable systematic effect.

Prompt gamma ray of carbon

Since the PVC sample was irradiated for a relatively long time the Doppler-broadened peak at 4441.0 keV from the ^{12}C(n,n')^{12}C reaction was also identified (see Fig. 2). It was exploited to confirm the result from our previous measurement on calcium carbonate ($CaCO_3$) [12]. A partial cross section of (12.8 ± 2.3) mb determined with Eq. (1) agrees well with that of (14.4 ± 3.3) mb derived in [12], thereby demonstrating reproducibility of our instrument. From our two measurements we derive an average value of (13.3 ± 1.9) mb for fast neutrons, compared to (2.6 ± 0.1) mb (4945.3-keV line of ^{12}C [28]) for thermal neutrons. Thus, in case of equal measurement conditions (i.e. same neutron flux and spectrometer set-up) FaNGaS offers greater sensitivity in the detection of carbon higher by a factor of approximately five.

Detection limit

The detection limit (DL) can be defined as the minimum mass of a pure element that has to be irradiated for a certain time in order to give a net signal with a certain standard deviation σ. For a certain counting time t_c, neglecting any neutron and gamma beam attenuation effects, it can be calculated with Eq. (1) from the minimum peak area $P_{E\gamma}(c)$ that might be estimated according to [42] as:

$$P_{E\gamma}(c) = \frac{\sqrt{2 \cdot B_{E\gamma}}}{c} \tag{7}$$

where $B_{E\gamma}$ is the area of the background below the gamma line of interest and c a predefined value for the relative uncertainty of the peak area.

For a counting live time of 12 h, the DL of cerium and chlorine were calculated for the most intense gamma line of each element by means of Eqs. (1) and (7). The value

Table 3 Prompt gamma rays of ^{136}Ce[a] and ^{140}Ce[b] induced by inelastic scattering of fast neutrons on $CeCl_3$

This work				From Demidov Atlas [14]		R
E_γ (keV)	$P_{E\gamma}(90°)/(\varepsilon_{E\gamma} f_{E\gamma}) \times 10^{-8}$ (count)	I_R(relative) (%)	$<\sigma_{E\gamma}(90°)>$ (mb)	E_γ (keV)	I_R(relative) (%)	
551.54 ± 0.08[c]	0.17 ± 0.02	0.40 ± 0.05	1230 ± 171	–	–	–
131.00 ± 0.04	1.29 ± 0.05	3.07 ± 0.16	20 ± 2	131.3 ± 0.4	3.3 ± 0.8	−0.28
241.63 ± 0.03	1.75 ± 0.06	4.17 ± 0.19	28 ± 2	241.91 ± 0.10	6.5 ± 0.7	−3.22
266.16 ± 0.03	2.24 ± 0.08	5.33 ± 0.25	35 ± 3	266.61 ± 0.10	6.2 ± 0.6	−1.34
306.38 ± 0.04	1.13 ± 0.05	2.69 ± 0.14	17.9 ± 1.6	306.91 ± 0.15	3.3 ± 0.3	−1.85
328.17 ± 0.04	1.81 ± 0.09	4.30 ± 0.25	29 ± 3	328.67 ± 0.15	5.9 ± 0.6	−2.46
431.85 ± 0.05[d]	0.96 ± 0.06	2.29 ± 0.16	15.2 ± 1.5	432.44 ± 0.15	3.0 ± 0.4	−1.65
486.35 ± 0.03[e]	13.6 ± 0.5	32 ± 1	215 ± 18	487.06 ± 0.05	37 ± 4	−1.10
520.38 ± 0.10[e,f]	0.24 ± 0.04	0.57 ± 0.09	3.81 ± 0.65	–	–	–
739.64 ± 0.12[g]	0.18 ± 0.02	0.42 ± 0.04	2.80 ± 0.35	740.0 ± 0.6	0.38 ± 0.15	0.26
751.15 ± 0.04	2.22 ± 0.07	5.27 ± 0.24	35 ± 3	751.65 ± 0.10	5.1 ± 0.5	0.31
815.32 ± 0.04	2.00 ± 0.06	4.76 ± 0.21	32 ± 3	815.84 ± 0.10	4.6 ± 0.5	0.29
867.52 ± 0.04[e]	2.99 ± 0.65	7.11 ± 1.56	47 ± 11	867.8 ± 0.2	6.5 ± 1.0	0.33
919.12 ± 0.05	0.85 ± 0.03	2.02 ± 0.10	13.5 ± 1.2	919.5 ± 0.2	2.1 ± 0.3	−0.25
924.83 ± 0.05[e]	1.13 ± 0.04	2.68 ± 0.12	17.8 ± 1.5	925.1 ± 0.2	2.9 ± 0.4	−0.53
950.60 ± 0.05	1.05 ± 0.04	2.50 ± 0.13	16.7 ± 1.5	950.84 ± 0.15	2.3 ± 0.2	0.86
982.22 ± 0.11[e]	0.25 ± 0.07	0.60 ± 0.16	4.01 ± 1.10	981.1 ± 0.4	0.64 ± 0.08	−0.21
1032.90 ± 0.36[h]	0.10 ± 0.03	0.24 ± 0.07	1.62 ± 0.49	–	–	–
1088.30 ± 0.13[e]	0.45 ± 0.15	1.07 ± 0.35	7.13 ± 2.39	–	–	–
1135.20 ± 0.26	0.18 ± 0.03	0.42 ± 0.06	2.80 ± 0.46	–	–	–
1232.84 ± 0.16	0.28 ± 0.03	0.66 ± 0.08	4.40 ± 0.62	1233.6 ± 0.4	0.7 ± 0.2	−0.18
1282.72 ± 0.19	0.12 ± 0.02	0.29 ± 0.05	1.91 ± 0.37	–	–	–
1303.20 ± 0.10	0.29 ± 0.03	0.69 ± 0.07	4.60 ± 0.55	1304.0 ± 0.8	0.8 ± 0.2	−0.52
1321.17 ± 0.60[h]	0.23 ± 0.04	0.53 ± 0.10	3.56 ± 0.70	–	–	–
1404.93 ± 0.09[f]	0.45 ± 0.03	1.08 ± 0.08	7.19 ± 0.74	–	–	–
1420.19 ± 0.21	0.11 ± 0.02	0.26 ± 0.05	1.74 ± 0.34	–	–	–
1474.71 ± 0.29[c,e,h]	0.13 ± 0.02	0.32 ± 0.05	2.12 ± 0.38	–	–	–
1525.70 ± 0.11	0.25 ± 0.02	0.58 ± 0.06	3.88 ± 0.47	1526.4 ± 0.5	0.49 ± 0.10	0.81
1539.86 ± 0.32[d,h]	0.09 ± 0.02	0.21 ± 0.06	1.39 ± 0.39	–	–	–
1565.14 ± 0.31[d]	0.11 ± 0.03	0.27 ± 0.06	1.82 ± 0.42	–	–	–
1595.98 ± 0.07	42 ± 1	100	666 ± 56	1596.20	100	–
1619.75 ± 0.32	0.10 ± 0.03	0.25 ± 0.07	1.65 ± 0.48	1620.5 ± 1.0	0.23 ± 0.08	0.16
1623.62 ± 0.16[g]	0.14 ± 0.02	0.33 ± 0.04	2.23 ± 0.32	–	–	–
1877.26 ± 0.16	0.27 ± 0.02	0.65 ± 0.05	4.34 ± 0.48	–	–	–
2051.08 ± 0.32	0.06 ± 0.02	0.14 ± 0.04	0.92 ± 0.25	–	–	–
2521.41 ± 0.14	0.43 ± 0.03	1.01 ± 0.07	6.73 ± 0.69	2521.3 ± 0.5	1.4 ± 0.2	−1.82
2546.63 ± 0.26	0.16 ± 0.02	0.38 ± 0.06	2.55 ± 0.42	2547.4 ± 0.8	0.57 ± 0.18	−0.99
2899.46 ± 0.14	0.46 ± 0.03	1.10 ± 0.07	7.30 ± 0.71	2900.1 ± 0.7	1.1 ± 0.2	−0.01
3118.15 ± 0.13[g]	0.39 ± 0.02	0.93 ± 0.06	6.20 ± 0.62	3120.4 ± 1.2[i]	0.56 ± 0.12	2.73
3319.29 ± 0.25	0.13 ± 0.02	0.31 ± 0.04	2.08 ± 0.31	–	–	–
3471.02 ± 0.24	0.16 ± 0.02	0.39 ± 0.04	2.60 ± 0.35	–	–	–
3643.53 ± 0.37[d]	0.09 ± 0.02	0.23 ± 0.05	1.50 ± 0.34	–	–	–

E_γ is the gamma-ray energy, $P_{E\gamma}(90°)/(\varepsilon_{E\gamma} f_{E\gamma})$ the net counts in the gamma-ray peak divided by the full-energy-peak efficiency and the gamma self-absorption factor, I_R the relative intensity of the gamma ray and $<\sigma_{E\gamma}(90°)>$ the fission-neutron spectrum-averaged partial cross section for gamma-ray production at an angle of 90° between neutron beam and detector determined with Eq. (1). R is the residual calculated by means of Eq. (6)

[a]Reaction threshold for inelastic scattering is 0.56 MeV [41]

Table 3 (continued)

[b]Reaction threshold for inelastic scattering is 1.61 MeV [29, 30]

[c]Gamma ray of ^{136}Ce

[d]Interference from ^{142}Ce(n,n'γ)^{142}Ce possible with respect to [27]

[e]Corrected for background interferences

[f]Doublet with ^{142}Ce (see Table 4)

[g]Corrected for escape peak interference

[h]Somewhat cautious assignment, as relative intensities differ considerably compared to data given in [26]

[i]Wrong level energy assigned by Demidov et al. [14]

Table 4 Prompt gamma rays of ^{142}Ce[a] induced by inelastic scattering of fast neutrons on $CeCl_3$

This work				From Demidov Atlas [14]		*R*
E_γ (keV)	$P_{E\gamma}$ (90°)/($\varepsilon_{E\gamma}$:$f_{E\gamma}$)×10^{-8} (count)	I_R (relative) (%)	$<\sigma_{E\gamma}$ (90°)> (mb)	E_γ (keV)	I_R (relative) (%)	
522.88 ± 0.08	0.25 ± 0.03	0.59 ± 0.08	32 ± 5	522.0 ± 0.3[b]	0.83 ± 0.15	1.31
577.46 ± 0.04	2.15 ± 0.09	5.11 ± 0.26	272 ± 24	578.1 ± 0.2	6.3 ± 0.8	−1.41
640.63 ± 0.03	10.6 ± 0.3	25.0 ± 1.1	1333 ± 112	641.23 ± 0.06	29 ± 3	−1.23
892.16 ± 0.13	0.23 ± 0.02	0.56 ± 0.06	30 ± 4	–	–	–
894.56 ± 0.05	1.29 ± 0.05	3.06 ± 0.15	163 ± 14	894.76 ± 0.15[c]	4.1 ± 0.5	−0.96
1011.07 ± 0.06	0.76 ± 0.03	1.81 ± 0.10	96 ± 9	1011.5 ± 0.3	2.6 ± 0.4	−1.91
1058.13 ± 0.27[d]	0.09 ± 0.03	0.21 ± 0.07	11.3 ± 3.8	1059.0 ± 0.15	0.63 ± 0.15[c]	−2.53
1243.20 ± 0.29[e]	0.10 ± 0.02	0.24 ± 0.06	12.6 ± 3.1	–	–	–
1362.36 ± 0.14	0.42 ± 0.03	0.99 ± 0.08	53 ± 6	–	–	–
1388.59 ± 0.17	0.12 ± 0.03	0.30 ± 0.07	15.7 ± 3.9	–	–	–
1402.36 ± 0.12	0.30 ± 0.02	0.71 ± 0.06	38 ± 4	1404.3 ± 0.3[f]	1.9 ± 0.2	−2.12
1478.43 ± 0.26[g]	0.14 ± 0.02	0.32 ± 0.05	17.1 ± 3.1	–	–	–
2004.15 ± 0.37	0.06 ± 0.02	0.15 ± 0.04	7.84 ± 2.03	–	–	–
2038.77 ± 0.34	0.09 ± 0.02	0.21 ± 0.04	11.3 ± 2.2	–	–	–
2186.63 ± 0.41	0.13 ± 0.02	0.31 ± 0.06	16.6 ± 3.4	–	–	–
2448.81 ± 0.19	0.09 ± 0.02	0.22 ± 0.04	11.8 ± 2.2	–	–	–

E_γ is the gamma-ray energy, $P_{E\gamma}$ (90°)/($\varepsilon_{E\gamma}$:$f_{E\gamma}$) the net counts in the gamma-ray peak divided by the full-energy-peak efficiency and the gamma self-absorption factor, I_R the relative intensity of the gamma ray and $<\sigma_{E\gamma}$ (90°)> the fission-neutron spectrum-averaged partial cross section for gamma-ray production at an angle of 90° between neutron beam and detector determined with Eq. (1). *R* is the residual calculated by means of Eq. (6)

[a]Threshold for inelastic scattering is 0.65 MeV [29, 30]

[b]520 and 523 keV

[c]892 and 895 keV

[d]Must be reviewed with caution, as a line at 1637 keV from the same excited level [20, 27] is not reported in [14]

[e]Probably from $E^* = 3423.61$ keV [27]; main line at 2782.2 keV in [20, 27] might have been not observed due to lower efficiency

[f]1402 and 1405 keV

[g]Corrected for background interference

of $B_{E\gamma}$ was determined from the beam background with HYPERMET-PC [19]. For a value of $c = 0.5$, corresponding to a peak area uncertainty of 50%, the smallest quantity of pure element that can be detected is 1 mg for cerium (^{140}Ce, $E_\gamma = 1596.0$ keV, $<\sigma_{E\gamma}(90°)> = 666$ mb) and 2 mg for chlorine (^{35}Cl, $E_\gamma = 1763.1$ keV, $<\sigma_{E\gamma}(90°)> = 70$ mb).

Conclusions

Emission of prompt gamma rays following fast-neutron inelastic scattering (n,n'), (n,p) and (n,α) reactions on a $CeCl_3$ and a PVC sample were measured with the FaNGaS instrument operated at MLZ. In total, 29 and 58 prompt

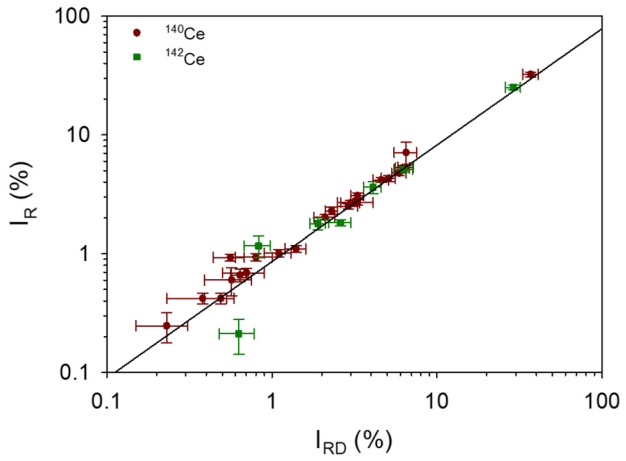

Fig. 7 Relationship between the relative intensities I_R of the prompt gamma rays induced by fast-neutron inelastic scattering (n,n') reactions on cerium measured in this work and the relative intensities I_{RD} tabulated in the Demidov Atlas [14]. The solid line represents the fit of the data with Eq. (5)

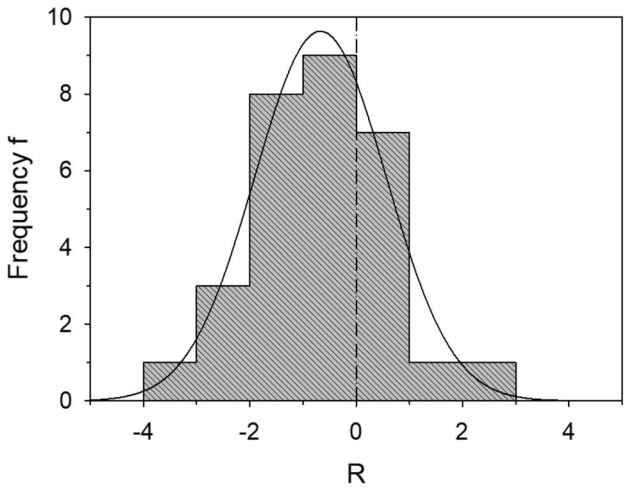

Fig. 8 Comparison of the relative intensities of the prompt gamma rays induced by fast-neutron inelastic scattering (n,n') reactions on cerium obtained in this work with the data tabulated in the Demidov Atlas [14] in the form of a histogram of the residuals R in units of standard deviation [σ] calculated with Eq. (6). The values of R are given in column 7 of Tables 3 and 4. The solid line represents the fit of the data with a Gaussian

gamma lines were identified for chlorine and cerium, respectively, and their relative intensities and fast-neutron spectrum-averaged partial gamma-ray production cross sections were determined. In comparison with the work of Demidov et al. [14], 37 gamma lines were detected additionally (10 for chlorine and 27 for cerium) owing to a better detector resolution and a higher mean excitation energy (2.30 MeV). However, 8 lines of chlorine and 14 lines of cerium, partly unassigned in [14], were not observed in our measurements either due to background interferences or lower sample-masses irradiated for a shorter time or were found to disagree with nuclear data provided in [20]. The relative intensities of the lines measured in our work agree reasonably well (1.3σ level for chlorine and 1.2σ level for cerium) with the values given in [14]. The detection limits of chlorine and cerium are determined as 2 and 1 mg, respectively, for a counting time of 12 h. In addition, the partial cross section of the 4.44-MeV line of carbon derived from the measurement of the PVC sample is found to be in good agreement with the value obtained in the previous measurement of $CaCO_3$ [12].

Funding Open Access funding enabled and organized by Projekt DEAL.

Declarations

Competing interests The authors have no competing interests to declare that are relevant to the content of this article.

References

1. Schrader CD, Stinner RJ (1961) Remote analysis of surfaces by neutron-gamma-ray inelastic scattering techniques. J Geophys Res 66:1951–1956
2. Jiggins AH, Habbani FI (1976) Prompt gamma-ray analysis using 3.29 MeV neutron inelastic scattering. Int J Appl Radiat Isot 27:689–693
3. Yates SW, Filo AJ, Cheng CY, Coope DF (1978) Elemental analysis by gamma detection following inelastic neutron scattering. J Radioanal Nucl Chem 46:343–355
4. Sowerby BD (1979) Elemental analysis by neutron inelastic scatter gamma rays with a radioisotope source. Nucl Instrum Methods 166:571–579
5. Ahmed MR, Demidov AM, Al-Najjar SA, Al-Amili MA (1974) Use of spectroscopy of gamma-radiation from the inelastic scattering of reactor fast neutrons for elemental analysis. J Radioanal Nucl Chem 23:199–203
6. Rossbach M, Genreith C, Randriamalala T, Mauerhofer E, Zs R, Kudejova P, Söllradl S, Belgya T, Szentmiklosi L, Firestone RB, Hurst AM, Bernstein L, Sleaford B, Escher JE (2015) TANDEM: a mutual cooperation effort for transactinide nuclear data evaluation and measurement. J Radioanal Nucl Chem 304:1359–1363

7. Randriamalala TH, Rossbach M, Mauerhofer E, Zs R, Söllradl S, Wagner FM (2016) FaNGaS: a new instrument for (n,n´γ) reaction measurements at FRM II. Nucl Instrum Methods A 806:370–377
8. Hable A, Ramsl C, Jericha E, Böck H, Randriamalala TH, Rossbach M (2017) FaNGaS: determination of integral fast fission cross sections (n,f) of 238U, 237Np, and 242Pu in a directed fission neutron beam at FRM II Garching. J Radioanal Nucl Chem. https://doi.org/10.1007/s10967-017-5512-7
9. Ilic Z, Mauerhofer E, Stieghorst C, Zs R, Rossbach M, Randriamalala TH, Brückel T (2020) Prompt gamma rays induced by inelastic scattering of fission neutrons on iron. J Radioanal Nucl Chem 325:641–645
10. Mauerhofer E, Ilic Z, Stieghorst C, Zs R, Rossbach M, Li J, Randriamalala TH, Brückel T (2021) Prompt and delayed gamma rays induced by epithermal and fast neutrons with indium. J Radioanal Nucl Chem 331:535–546
11. Mauerhofer E, Ilic Z, Stieghorst C, Zs R, Vezhlev E, Ophoven N, Randriamalala TH, Brückel T (2022) Prompt gamma rays from fast neutron inelastic scattering on aluminum, titanium and copper. J Radioanal Nucl Chem 331:3987–4000
12. Ophoven N, Ilic Z, Mauerhofer E, Randriamalala TH, Vezhlev E, Stieghorst C, Zs R, Brückel T, Jolie J, Strub E (2022) Fast neutron induced gamma rays from (n,n'), (n,p) and (n,α) reactions on $CaCO_3$. J Radioanal Nucl Chem 331:5729–5740
13. Wagner F, Kneschaurek P, Kastenmüller A, Loeper-Kabasakal B, Kampfer S, Breitkreutz H, Waschkowski W, Molls M, Petry W (2009) The munich fission neutron therapy facility MEDAPP at the research reactor FRM II. Strahlenther Onkol. https://doi.org/10.1007/s00066-008-1878-3
14. Demidov A, Govor L, Cherepantsev M, Ahmed S, Al-Najjar M, Al-Amili N, Al-Assafi N, Rammo N (1978) Atlas of gamma-ray spectra from the inelastic scattering of reactor fast neutrons. Atomizdat, Moscow
15. Bernstein L, Brown D, Basunia S, Hurst A, Kawano T, Kelley J, Kondev F, McCutchan E, Nesaraja C, Slaybaugh R, Sonzogni A, (2015) Nuclear data needs and capabilities for applications. In: White paper LLNL report LLNL-CONF-676585. http://bang.berkeley.edu/events/ndnca/whitepaper
16. Romano C, Ault T, Bernstein L, Bahran R, Talou P, Quiter B, Pozzi S, Devlin M, Burke J, Bredeweg T, McCutchan E, Stave S, Bailey T, Hogle S, Chapman C, Hurst A, Nelson N, Tovesson F, Hornback D, (2018) Proceedings of the nuclear data roadmapping and enhancement workshop (NDREW) for nonproliferation. In: White paper ORNL/LTR-2018/510. https://info.ornl.gov/sites/publications/Files/Pub111600.pdf
17. Bernstein L, Romano C, Brown D, Casperson R, Descalle MA, Devlin M, Pickett C, Rearden B, Vermeulen C, (2019) Final report for the workshop for applied nuclear data activities (WANDA). In: White Paper LLNL-PROC-769849
18. Hurst AM, Bernstein LA, Kawano T, Lewis AM, Song K (2021) The Baghdad Atlas: a relational database of inelastic neutron scattering (n,n´γ) data. Nucl Instrum Meth A 995:165095
19. Zs R, Belgya T, Molnár GL (2005) Application of Hypermet-PC in PGAA. J Radioanal Nucl Chem 265:261–265
20. NuDat 3.0 national nuclear data center. Brookhaven National Laboratory. https://www.nndc.bnl.gov/nudat3/
21. Chen J, Cameron J, Singh B (2011) Nuclear data sheets for A= 35. Nucl Data Sheets 112:2715–2850
22. Cameron J, Chen J, Singh B, Nica N (2012) Nuclear data sheets for A= 37. Nucl Data Sheets 113:365–514
23. Ouellet C, Singh B (2011) Nuclear data sheets for A= 32. Nucl Data Sheets 112:2199–2355
24. Mccutchan EA (2011) Nuclear data sheets for A= 136. Nucl Data Sheets 152:331–667
25. Chen J (2017) Nuclear data sheets for A= 138. Nucl Data Sheets 146:1–386
26. Nica N (2018) Nuclear data sheets for A= 140. Nucl Data Sheets 154:1–403
27. Johnson TD, Symochko D, Fadil M, Tuli JK (2011) Nuclear data sheets for A= 142. Nucl Data Sheets 112:1949–2127
28. Zs R, Firestone RB, Belgya T, Molnár, (2004) Prompt Gamma-ray spectrum. In: Molnár GL (ed) Handbook of prompt gamma activation analysis with neutron beams. Kluwer Academic Publishers, Dordrecht/Boston/New York, pp 173–364
29. Nuclear Data Center (1996) Japan atomic energy agency, tables of nuclear data. https://wwwndc.jaea.go.jp/jendl/j40/j40.html
30. Shibata K, Iwamoto O, Nakagawa T, Iwamoto N, Ichihara A, Kunieda S, Chiba S, Furutaka K, Otuka N, Ohsawa T, Murata T, Matsunobu H, Zukeran A, Kamada S, Katakura J (2010) JENDL-4.0: a new library for nuclear science and engineering. J Nucl Sci Technol 48(1):1–30
31. Initial MCNP6 release overview MCNP6 version 1.0, Los Alamos national laboratory report LA-UR-13–22934
32. Goorley T et al (2017) Initial MCNP6 release overview. Nucl Technol 180:298–315
33. Conlin JL, Haeck W, Neudecker D, Parsons DK, White MC (2018) Release of ENDF/B-VIII.0-based ACE data files, Los Alamos national laboratory report LA-UR-18–24034 https://nucleardata.lanl.gov/files/la-ur-18-24034.pdf
34. Brown DA et al (2018) ENDF/B-VIII.0: the 8th major release of the nuclear reaction data library with CIELO-project cross sections, new standards and thermal scattering data. Nucl Data Sheets 148:1–142
35. Reilly D et al. (1991) Passive nondestructive assay of nuclear materials. https://www.lanl.gov/orgs/n/n1/FMTTD/neut_mc/pdfs/LA_UR_90_0732.pdf
36. NIST XCOM: photons cross sections database. National Institute of Standards and Technolog. https://physics.nist.gov/PhysRefData/Xcom/html/xcom1.html
37. Berger MJ, Hubbell JH, Seltzer S, Chang J, Coursey JS, Sukumar R, Zucker DS (2009) XCOM: photon cross sections database. NIST Stand Ref Database 8:87–3597
38. Barzilov A, Womble P (2014) Study of Doppler broadening of gamma-ray spectra in 14-MeV neutron activation analysis. J Radioanal Nucl Chem 301:811–819
39. Catz AL, Amiel S (1967) Study of lifetimes of nuclear levels by Doppler broadening attenuation using a (Ge)Li gamma-ray spectrometer. Nucl Phys A 92:222–232
40. OECD NEA Data Bank (2020) JANIS book of neutron-induced cross-sections. https://www.oecd-nea.org/janis/book/book-neutron-2020-09.pdf
41. Evaluated Nuclear Data File (ENDF) Database Version of 2022–10–07, International atomic energy agency (IAEA). https://www-nds.iaea.org/exfor/endf.htm
42. Zs R (2009) Determining elemental composition using prompt γ activation analysis. Anal Chem. https://doi.org/10.1021/ac901705